PCCP

Accepted Manuscript

ROYAL SOCIETY OF CHEMISTRY

www.rsc.org/pccp

Journal Name

RSCPublishing

ARTICLE

Charge-transfer complex versus σ-complex between TiO_2 and bis(dicyanomethylene) electron acceptors

Cite this: DOI: 10.1039/x0xx00000x

Jun-ichi Fujisawa,*[1] Morio Nagata,[2] and Minoru Hanaya[1]

Received 00th January 2012,
Accepted 00th January 2012

DOI: 10.1039/x0xx00000x

www.rsc.org/

A novel group of organic-inorganic hybrid material is created by combination of titanium dioxide (TiO_2) nanoparticles with bis(dicyanomethylene) (TCNX) electron acceptors. The TiO_2-TCNX complex is produced by nucleophilic addition reactions between a hydroxy group on TiO_2 surface and TCNX with the formation of a σ-bond between them. The nucleophilic addition reaction generates a negatively-charged diamagnetic TCNX adsorbate that serves as an electron donor. The σ-bonded complex characteristically shows visible-light absorption due to interfacial charge-transfer (ICT) transitions. In this paper, we report on another kind of complex formation between TiO_2 and TCNX. We have systematically studied the structures and visible-light absorption properties of the TiO_2-TCNX complexes with changing the electron affinity of TCNX. We found that TCNX acceptors with lower electron affinities form charge-transfer complexes with TiO_2 without the σ-bond formation. The charge-transfer complexes show strong visible-light absorption due to interfacial electronic transitions with little charge-transfer nature, which are different from the ICT transitions in the σ-bond complexes. The charge-transfer complexes induce efficient light-to-current conversions due to the interfacial electronic transitions, revealing the high potential for applications to light-energy conversions. Furthermore, we demonstrate that the formations of the two kinds of complexes are selectively controlled with the electron affinity of TCNX.

Introduction

Titanium dioxide (TiO_2) is a wide-band-gap semiconductor with high photocatalytic activities and carrier transportabilities.[1,2] For photocatalytic and photovoltaic energy conversions based on TiO_2, the enhancement of the visible-light absorption and efficient charge separation of photocarriers are important subjects. Because of the electron-accepting property, so far, TiO_2 has been combined with electron-donating light absorbers such as dyes.[1,2] Recently, we discovered a novel type of TiO_2-organic hybrid material formed by combination with organic electron acceptors.[3-8] We observed the peculiar coloration of TiO_2 (anatase) nanoparticles due to immersion in the solution of bis(dicyanomethylene) (TCNX) electron acceptors[9]. As shown in Fig. 1(a), TiO_2 nanoparticles is strongly coloured by immersion in the pale yellow solution of 7,7,8,8-tetracyanoquinodimethane (TCNQ). As shown in the right of Fig. 1(a), the TiO_2-TCNQ complex shows a broad visible-light absorption band in the longer-wavelength region than the inter-band transitions in TiO_2 and intra-molecular

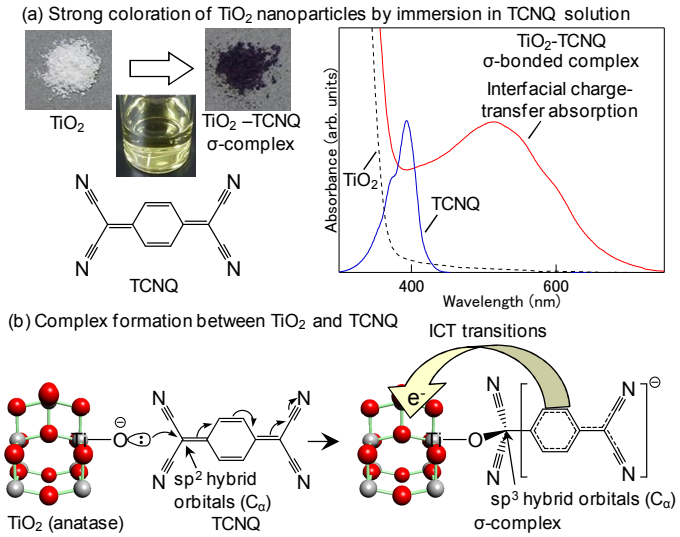

Fig. 1. (a) Coloration of TiO_2 nanoparticles by immersion in TCNQ solution and the appearance of a broad ICT band and (b) formation mechanism of the TiO_2-TCNQ σ-complex by a nucleophilic addition reaction. The experimental data were reported in Ref. 5.

transitions in TCNQ.[3-8] Similar coloration was reported in 1971 by Hosaka *et al.*[10] Once they reported that the peculiar coloration is attributed to TCNQ anion radicals, but in 1982 they found that almost all of TCNQ species adsorbed on TiO_2 are diamagnetic, denying their previous presumption.[11] Since then the TiO_2-TCNQ complex and the mechanism of the coloration had not been unravelled. Our experimental and theoretical analyses of the vibrational spectrum revealed that the TiO_2-TCNQ complex is produced by a nucleophilic addition reaction of a deprotonated hydroxy group on TiO_2 with TCNX, as shown in Fig. 1(b). By the nucleophilic addition reaction, a negatively-charged diamagnetic σ-bonded complex is generated on TiO_2. The negatively charged TCNX moiety serves as an electron donor, not as an acceptor, in contrast to free TCNQ. The broad visible-light absorption was assigned to interfacial charge-transfer (ICT) transitions from the negatively charged TCNX moiety to the conduction band of TiO_2, as shown in Fig. 1(b).[3-8] It is suggested from the mechanism of the complex formation that the σ-bond formation originates from the high electron affinity of TCNQ and the σ-complex is not formed with weaker TCNX acceptors. From this perspective, we have studied the σ-complex formation with changing the electron affinity of TCNX. Our recent experiments showed that the presumption is correct, but another type of complex is formed between TiO_2 and TCNX with lower electron affinities. The complex is assigned to a charge-transfer complex without the σ-bond formation, which is apparently distinguished from the σ-complex for the reason that the form complex is not stabilized by σ-bond formation, but by charge-transfer interactions.[11] In this paper, we report the formation of the charge-transfer complex. The charge-transfer complex shows a strong visible-light absorption due to an interfacial electronic transition with little charge-transfer nature, which is different from the ICT transition of the σ-complex. In addition, the charge-transfer complex performs efficient light-to-current conversions due to the interfacial transitions. Furthermore, our work demonstrates that the formations of the two kinds of complexes are selectively controlled with the electron affinity of TCNX.

In our experiments, two kinds of TCNX electron acceptors were employed in addition to TCNQ. They are 11,11,12,12-tetracyanonaphtho-1,4-quinodimethane (1,4-TCNAQ) and 6,6,7,7-tetracyanothieno-2,5-quinodimethane (TCNTQ), as shown in Fig. 2(a). The redox potentials of 1,4-TCNAQ and TCNTQ are +0.07 V and +0.02 V vs SCE, respectively, which are lower than that (+0.22 V) of TCNQ.[12] This data indicate that these TCNXs are weaker electron acceptors than TCNQ.

Experimental

1,4-TCNAQ and TCNTQ were synthesized according to the procedure described in Electronic Supporting Information (ESI). TCNQ was purchased from Tokyo Chemical Industry and used without further purification. For measurements of the absorption spectra of the TiO_2-TCNX complexes, thin layer

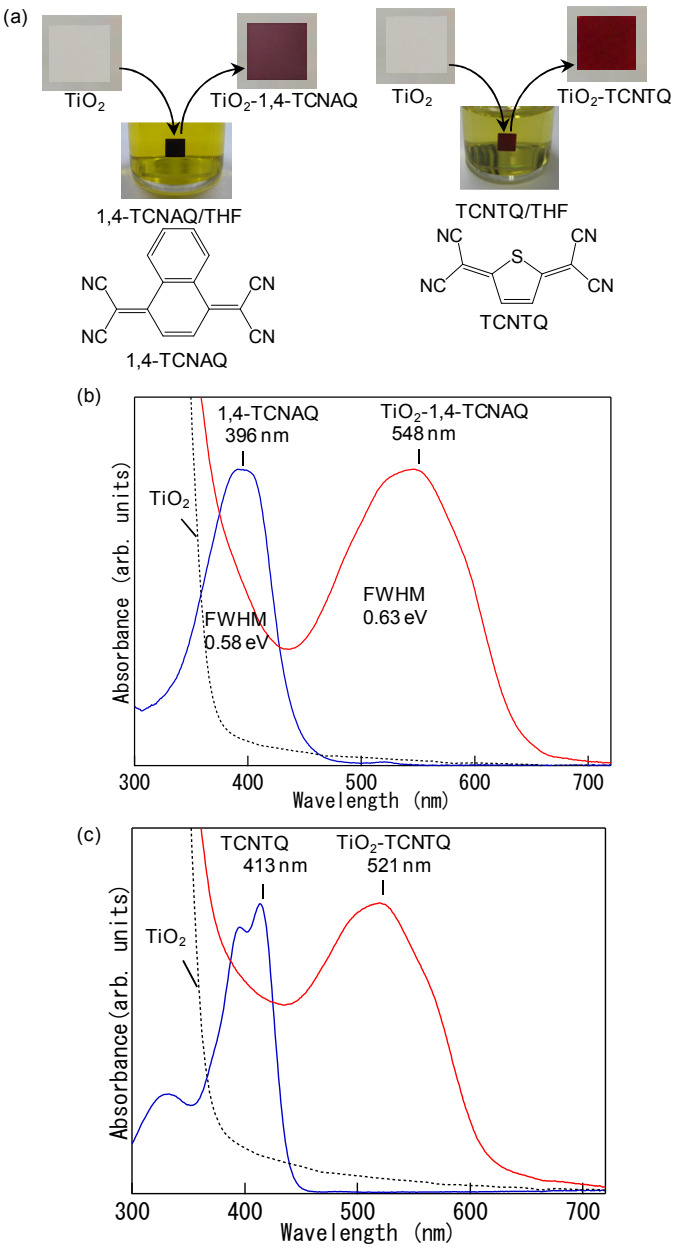

Fig. 2. (a) Colorations of TiO_2 mesoporous films by immersion in the solutions of 1,4-TCNAQ and TCNTQ and near-UV-visible absorption spectra of TiO_2 mesoporous films immersed in the (b) 1,4-TCNAQ (red) and (C) TCNTQ (red) solutions together with those of TiO_2 (dashed black curve), 1,4-TCNAQ (blue) and TCNTQ (blue).

samples were prepared by the following method. At first, mesoporous TiO_2 (anatase) films (thickness: ca. 6 μm) were fabricated by screen-printing of TiO_2 nanoparticle paste (T/SP, Solaronix SA Co.) several times on quartz glass substrates and sintering them at 773 K for 30 min. Then, the sintered TiO_2 films were immersed in the TCNX solutions (solvent: tetrahydrofran for 1,4-TCNAQ and TCNTQ and acetonitrile for TCNQ) at room temperature for 24 hours. The absorption spectra of the film samples were measured by means of a UV-Visible-NIR spectrophotometer (Shimadzu Co., UV-3600). For measurements of the FT-IR spectra of the TiO_2-TCNX

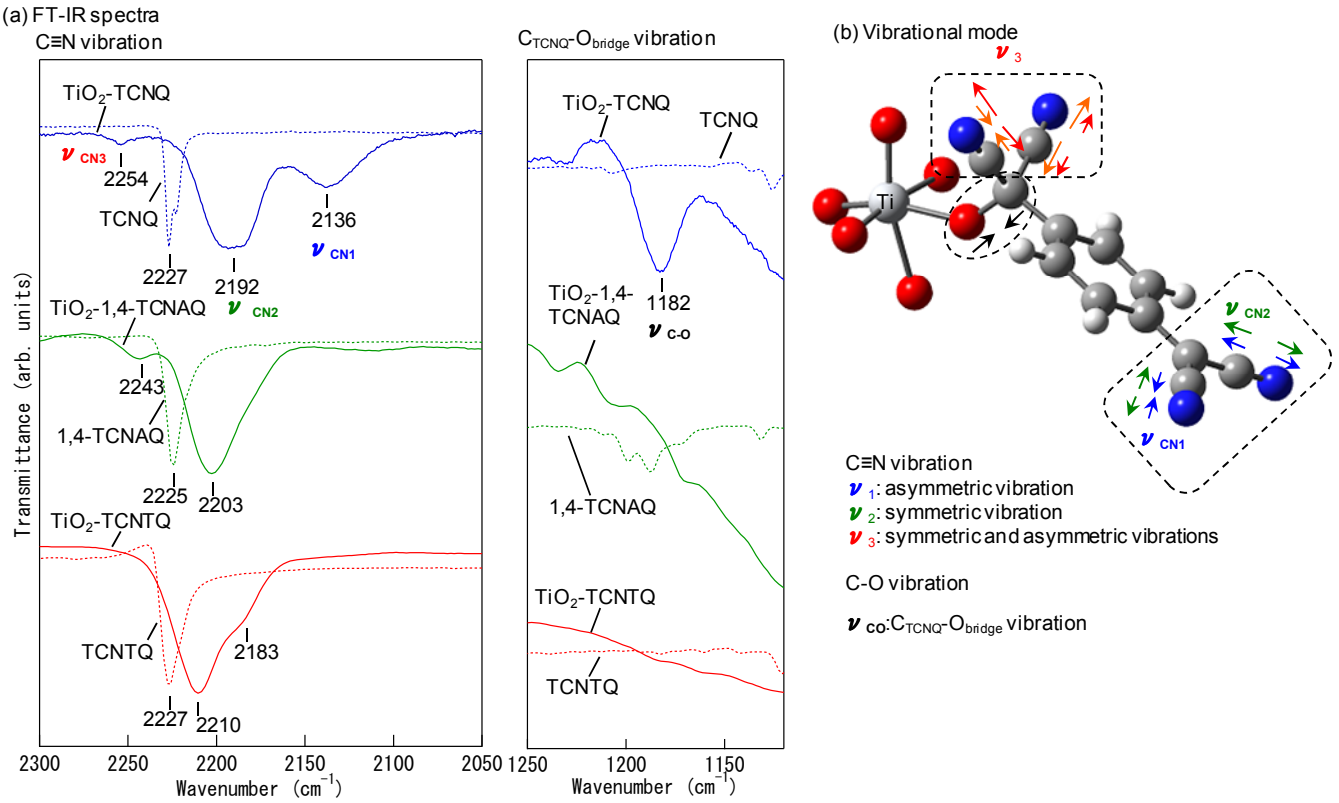

Fig. 3. (a) FT-IR spectra (solid curves) of TiO_2-TCNQ (blue), TiO_2-1,4-TCNAQ (green), and TiO_2-TCNTQ (red) complexes together with those (dashed curves) of TCNQ (blue), 1,4-TCNAQ (green), and TCNTQ (red) and (b) C≡N and C_{TCNQ}-O_{bridge} vibrational modes in the TiO_2-TCNQ complex. The scale of the vertical axis in the right spectra is the same as that of the left ones. Gray: carbon atom, white: hydrogen atom, red: oxygen atom, and large white: titanium atom.

complexes, powder samples were prepared by the following method. TiO_2 (anatase) nanoparticles (P90, Aerosil) were immersed in the TCNX solutions (solvent: tetrahydrofran for 1,4-TCNAQ and TCNTQ and acetonitrile for TCNQ) at room temperature for 24 hours. Then, the immersed powders were filtered and washed and then vacuum-dried. The FT-IR spectra of the powder samples were measured by means of an FT-IR spectrometer (Shimadzu, IRPrestige-21).

Electrochemical photovoltaic cells were fabricated by the following method. Mesoporous TiO_2 electrodes (active area: 4×4 mm^2) were prepared by screen-printing of four kinds of TiO_2 nanoparticle pastes, HT/SP, T/SP, D/SP, and R/SP (Solaronix SA Co.) with different particle sizes on F-doped SnO_2 (FTO) transparent conducting glass substrates (Nippon Sheet Glass Co.) with sheet resistance of 10 Ω per square and sintering them at 773 K for 30 min. The sintered TiO_2 electrodes were treated by $TiCl_4$ for improvement of electric contacts between nanoparticles and rinsed with deionized water and ethanol, then sintered at 773 K for 30 min again. The thickness of the TiO_2 electrodes was set to ca. 18 μm. The TiO_2-1,4-TCNAQ photoelectrode was fabricated by immersing the TiO_2 electrode in the 3 mM 1,4-TCNAQ solution (solvent: tetrahydrofran) that includes colorless 6-methoxy-2-naphthoic acid (1 mM) as a coadsorbent at room temperature for 48 hours. The TiO_2-TCNTQ photoelectrode was fabricated by immersing the TiO_2 electrode in the 0.1 mM TCNX solution (solvent: tetrahydrofran) that includes colorless ursocholic acid (1 mM) as a coadsorbent at room temperature for 24 hours. The coadsorbents were used for suppression of back electron-transfer reactions from TiO_2 to the iodide electrolyte by covering vacant surfaces on TiO_2. Photovoltaic cells were fabricated using the TiO_2-TCNX photoelectrode, a Pt-spattered FTO glass counter electrode, I^-/I_3^- redox couple electrolyte (solvent: acetonitrile), and a polymer spacer film (thickness: 30 μm, Surlyn®film). The iodide electrolyte for the TiO_2-1,4-TCNAQ photovoltaic cell includes 0.2M LiI, 0.025M I_2, 0.1M guanidinium thiocyanate, and 0.2M tetra-*n*-butylammonium iodide and the one for the TiO_2-TCNTQ photovoltaic cell includes 1M LiI and 0.025M I_2. Excitation spectra of incident photon-to-current conversion efficiencies (IPCE) were measured by means of a Hypermonolight system (SM-250E, Bunkoukeiki) with a calibrated silicon photodiode (S1337, Bunkoukeiki).

Computational

Optimized structures, energies and electronic distributions of molecular orbitals (Kohn-Sham energy eigenstates), and electronic-excitation spectra were calculated by DFT[13] and TD-DFT[14] calculations with the widely employed B3LYP functional[15,16] and 6-31G+(d,p)[17,18] basis set. We have already

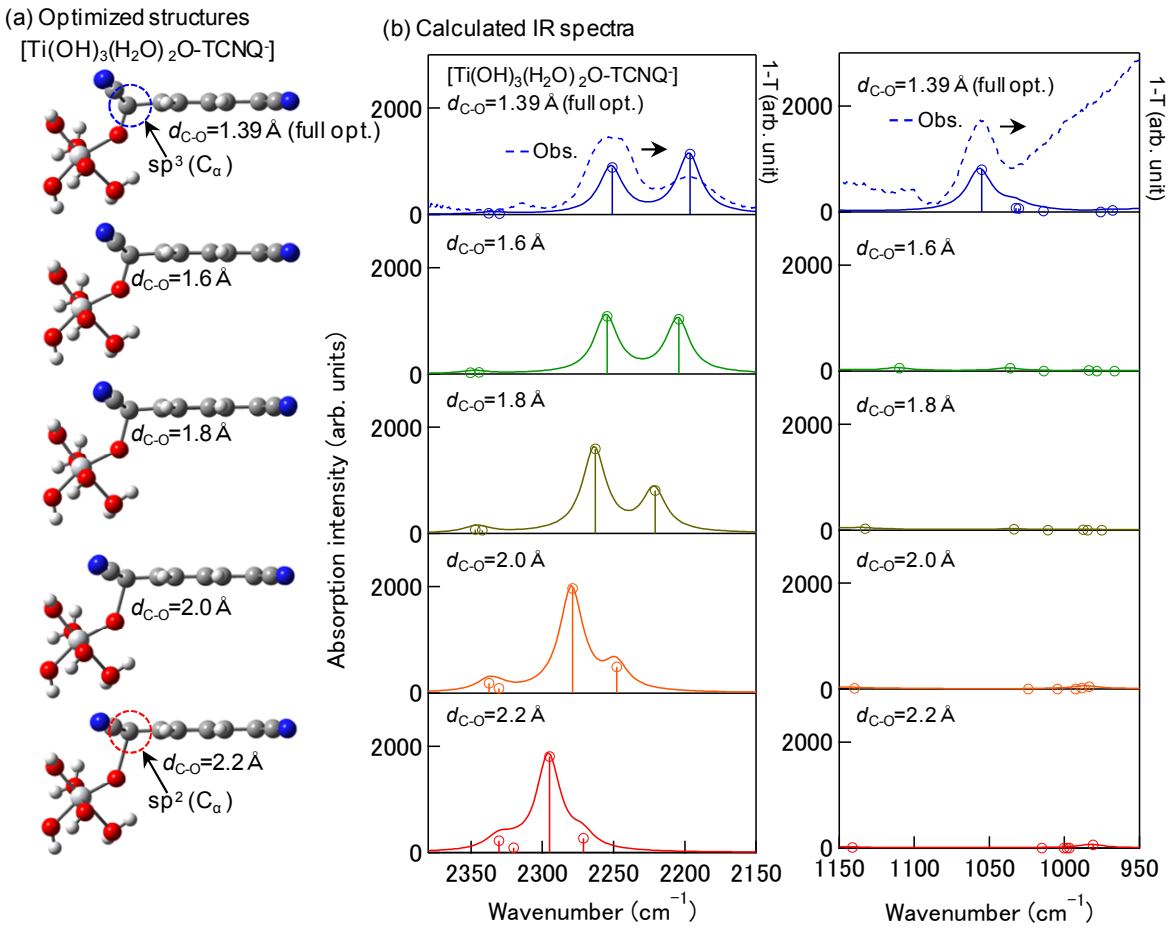

Fig. 4. (a) Optimized structures with different C_{TCNQ}-O_{bridge} bond lengths and (b) their calculated vibrational absorption spectra of [Ti(OH)$_3$(H$_2$O)$_2$O-TCNQ$^-$]. The vibrational curves were obtained by convolution of the line spectra with gaussian functions with FWHM of 20 cm^{-1}. The blue dashed curves are experimental data in Fig. 3(a). The experimental wavenumber values are blue-shifted by 60 cm^{-1} for the C≡N vibrational spectrum and red-shifted by 127 cm^{-1} for the C_{TCNQ}-O_{bridge} vibrational spectrum for purposes of comparison to the calculated spectra. Gray: carbon atom, white: hydrogen atom, red: oxygen atom, and large white: titanium atom.

confirmed the validity of the functional in the calculations of the TiO_2-TCNQ complex.[7,8] Solvation effects of acetonitrile for TCNQ and tetrahydrofuran for 1,4-TCNAQ and TCNTQ were taken into account with the conductor-like polarizable continuum model (CPCM)[19,20], since CPCM is one of successful solvation models.[21] In order to examine the functional dependence, DFT and TD-DFT calculations were also performed by employing the CAM-B3LYP functional[22] with the long range correction. We confirmed that qualitatively similar results are obtained with the CAM-B3LYP functional. All the calculations were performed by using a Gaussian 09 software.[23]

Results and discussion

Formation of charge-transfer complexes

As shown in Fig. 2(a), TiO_2 (anatase) mesoporous films were intensely coloured by immersion in the 1,4-TCNAQ and TCNTQ solutions. The developed colours are apparently different from those (yellow) of the corresponding TCNX compounds. As shown in Fig. 2(b), the TiO_2 film immersed in the 1,4-TCNAQ solution shows a absorption band at 548 nm. This absorption band is apparently different from the intra-molecular absorption band at 396 nm of 1,4-TCNAQ. Similarly, the TiO_2 immersed in the TCNTQ solution shows an absorption band at 521 nm, which is different from the intra-molecular absorption band at 413 nm in TCNTQ. The strong colorations and the appearance of the visible-light absorption bands indicate complex formations of 1,4-TCNAQ and TCNTQ with TiO_2 in spite of the lower electron affinities than TCNQ. However, a certain difference between those absorption bands and the ICT band of the TiO_2-TCNQ complex was found. Usually, ICT absorption bands rise up gradually reflecting the gradually increasing density-of-states of the conduction band of TiO_2 and unoccupied surface states below the conduction-band edge (CBE), as shown in Fig. 1(a).[24-26] In contrast, the absorption bands observed for the TiO_2-1,4-TCNAQ and TiO_2-TCNTQ complexes rise up more sharply than the ICT band of the TiO_2-TCNQ σ-complex. In addition, the band-widths of the absorption bands are considerably narrower than that of the ICT band (Fig. 1(a)). For example, the full width at a half maximum

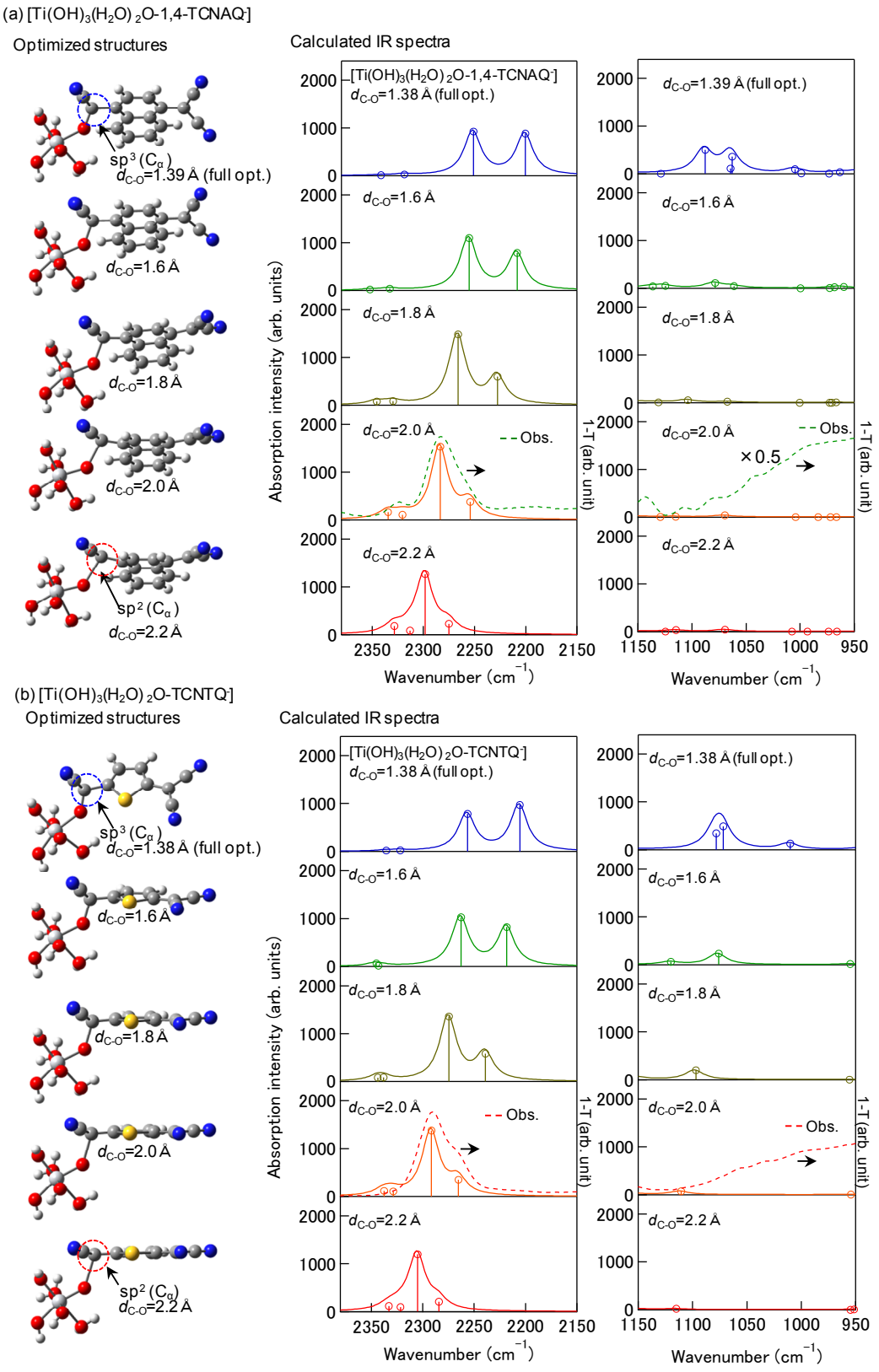

Fig. 5. Optimized structures (left) with different C_{TCNQ}-O_{bridge} bond lengths and their calculated vibrational absorption spectra (right) of (a) $[Ti(OH)_3(H_2O)_2O$-1,4-TCNAQ$^-]$ and (b) $[Ti(OH)_3(H_2O)_2O$-TCNTQ$^-]$. The vibrational curves were obtained by convolution of the line spectra with gaussian functions with FWHM of 20 cm^{-1}. The green and red dashed curves are experimental data in Fig. 3(a). The experimental wavenumber values are blue-shifted by 80 cm^{-1} for the C≡N vibrational spectra and red-shifted by 127 cm^{-1} for the C_{TCNQ}-O_{bridge} vibrational spectra for purposes of comparison to the calculated spectra. Gray: carbon atom, white: hydrogen atom, red: oxygen atom, yellow: sulfur atom, and large white: titanium atom.

(FWHM) of the absorption band of the TiO_2-1,4-TCNAQ complex was estimated to be 0.63 eV. This value is comparable to that (0.58 eV) of the intra-molecular band of 1,4-TCNAQ. This result suggests that the observed visible-light absorption bands might not be attributed to ICT transitions.

Fig. 3(a) shows FT-IR spectra of the TiO_2-TCNQ, -1,4-TCNAQ, and -TCNTQ complexes together with those of the corresponding free TCNX acceptors. The TiO_2-TCNQ complex shows three C≡N vibrational peaks at 2136, 2192, and 2254 cm^{-1}, which are widely split as compared to the almost single-peak structure of free TCNQ at 2227 cm^{-1}. The low-energy peaks at 2136 and 2192 cm^{-1} are attributed to the asymmetric and symmetric C≡N vibrations in the dicyanomethylene group far from the Ti-O_{bridge}-C_{TCNQ} bonding site, respectively, and the high-energy weak peak at 2254 cm^{-1} is due to the unresolved asymmetric and symmetric C≡N vibrational peaks in the dicyanomethylene group near the Ti-O-C bonding site, as reported in our previous paper, as shown in Fig. 3(b).[4] The large splitting is attributed to the large structural change from planar (sp^2 hybrid orbitals) to tetragonal (sp^3 hybrid orbitals) at the C_α atom (Fig. 1(a)) by the σ-bond formation. In contrast, the splittings of the C≡N vibrational peaks observed for the TiO_2-1,4-TCNAQ and TiO_2-TCNTQ complexes are much weaker than that in TiO_2-TCNQ. The former complex exhibits two vibrational peaks at 2203 and 2243 cm^{-1}. The latter complex shows a peak at 2210 cm^{-1} with a weak shoulder at ca. 2183 cm^{-1}. In addition, the TiO_2-TCNQ complex shows a C_{TCNQ}-O_{bridge} vibrational peak at 1182 cm^{-1}, which evidently indicates the σ-bond formation between TiO_2 and TCNQ. On the other hand, the latter two complexes exhibit no C_{TCNQ}-O_{bridge} vibrational peak. These results indicate that the structures of 1,4-TCNAQ and TCNTQ on TiO_2 are much different from that of the TiO_2- and TCNQ σ-complex and the σ-bond is not formed between 1,4-TCNAQ and TCNTQ and TiO_2.

Analyses of vibrational and electronic-excitation spectra

The observed vibrational spectra of the TiO_2-TCNQ, -1,4-TCNAQ and -TCNTQ complexes were examined by DFT calculations. In the calculations, mononuclear Ti model complexes, [$Ti(OH)_3(H_2O)_2$O-TCNQ$^-$], [$Ti(OH)_3(H_2O)_2$O-1,4-TCNAQ$^-$] and [$Ti(OH)_3(H_2O)_2$O-TCNTQ$^-$] were employed for the TiO_2-TCNQ, -1,4-TCNAQ, and -TCNTQ complexes, respectively, as shown in Fig. 4(a) and 5. Such model complexes have been confirmed to be suitable for analyses of the surface structures of the TiO_2-TCNX complexes.[7,8] The top picture in Fig. 4(a) displays the fully optimized structure with a C_{TCNQ}-O_{bridge} bond length equal to 1.39006 Å having a tetragonal conformation of the C_α atom. The structures shown below are optimized structures with different C_{TCNQ}-O_{bridge} bond lengths. Since the structural optimizations were not well converged with relaxations of all the hydroxy and water ligands, the coordinates of all the hydroxy and water ligands were fixed to those of the fully optimized structure. As shown in Fig. 4(a), the structure of the σ-complex changes from the tetragonal to a planar structure with increasing the C_{TCNX}-O_{bridge} bond length.

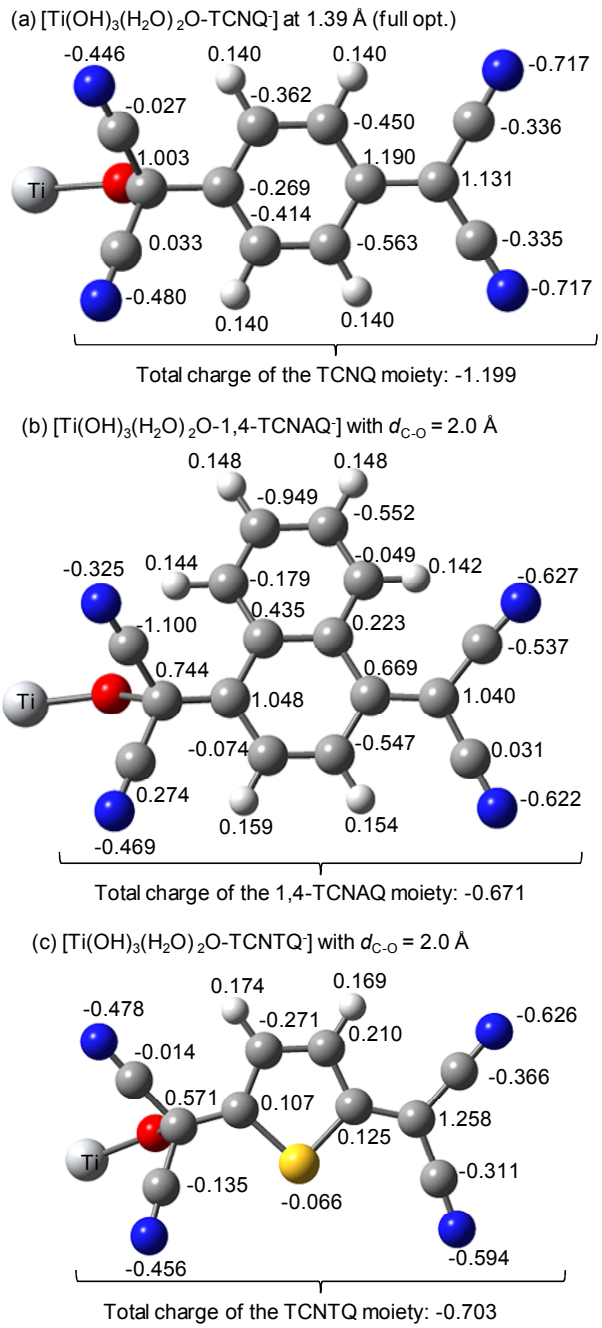

Fig. 6. Charge distributions of (a) [$Ti(OH)_3(H_2O)_2$O-TCNQ$^-$] fully optimized, (b) [$Ti(OH)_3(H_2O)_2$O-1,4-TCNAQ$^-$] and (c) [$Ti(OH)_3(H_2O)_2$O-TCNTQ$^-$] optimized with the C_{TCNX}-O_{bridge} bond length equal to 2.0 Å.

As shown in Fig. 4(b), the C≡N splitting is remarkably shrunk with the increase in the C_{TCNQ}-O_{bridge} bond length. At 2.0 and 2.2 Å, the C≡N vibrational spectra become a single-peak spectrum with two shoulders. In addition, the C_{TCNQ}-O_{bridge} vibrational peak disappears at the bond lengths longer than 1.6 Å. These changes are reasonable, because the structure of TCNQ almost changes from the tetragonal to planar one with the increase of the C_{TCNQ}-O_{bridge} bond length. The experimental spectra (blue dashed curves) observed for the TiO_2-TCNQ complex are in qualitatively good agreement with the calculated

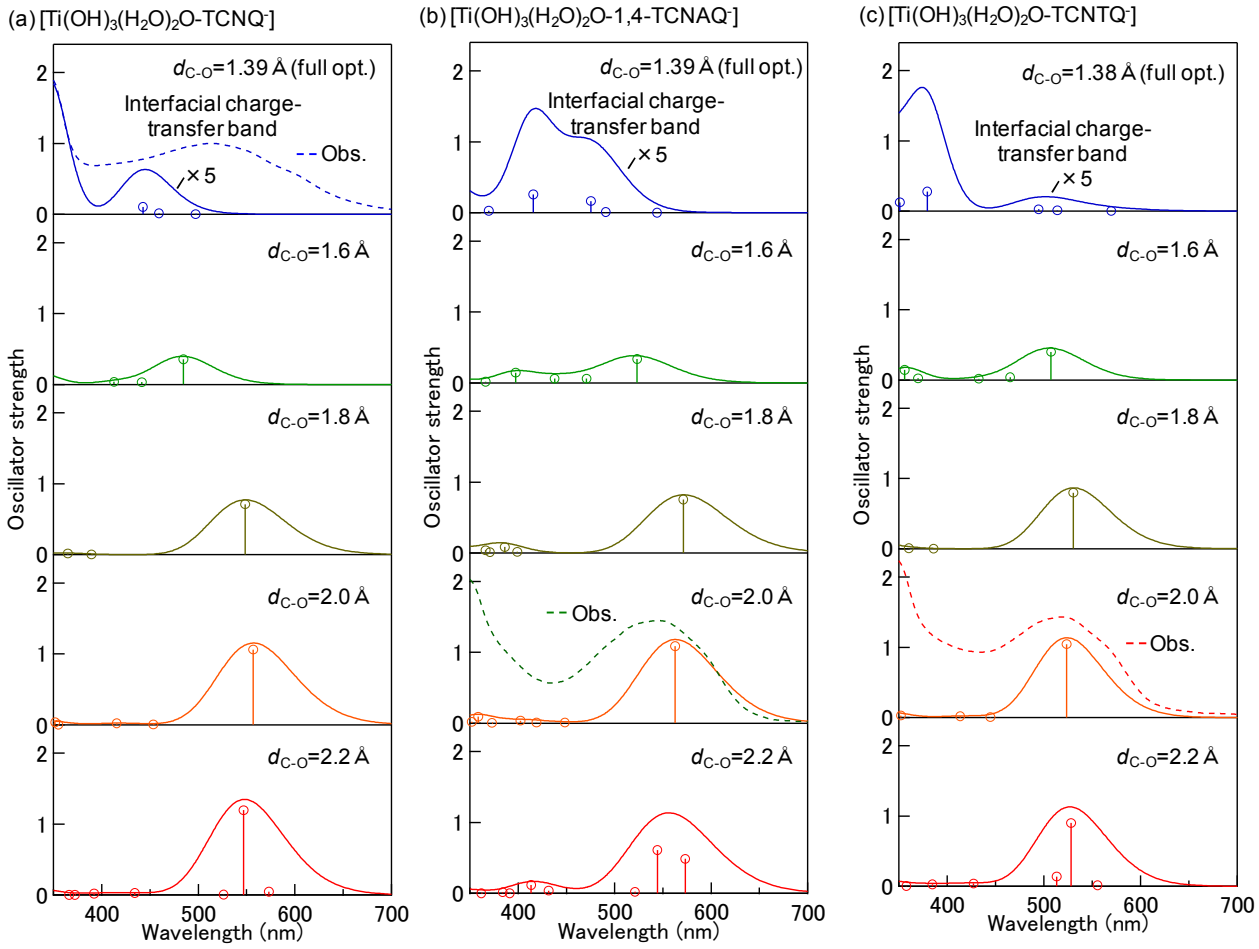

Fig. 7. Calculated electronic-excitation spectra of (a) [Ti(OH)$_3$(H$_2$O)$_2$O-TCNQ$^-$], (b) [Ti(OH)$_3$(H$_2$O)$_2$O-1,4-TCNAQ$^-$], and (c) [Ti(OH)$_3$(H$_2$O)$_2$O-TCNTQ$^-$]. The spectra were obtained by convolution of the line spectra with gaussian functions with FWHM of 3000 cm^{-1}. The blue, green and red dashed curves are experimental data in Fig. 1(a), 2(b) and 2(c).

C≡N and C_{TCNX}-O_{bridge} vibrational spectra (blue solid curves) of the fully optimized structure with the σ-bond, confirming the reported assignment.[3-8]

Fig. 5(a) shows calculated optimized structures of [Ti(OH)$_3$(H$_2$O)$_2$O-1,4-TCNAQ$^-$] with different C_{TCNX}-O_{bridge} bond lengths and their vibrational spectra. As shown in the left figure, the fully optimized structures of [Ti(OH)$_3$(H$_2$O)$_2$O-1,4-TCNAQ$^-$] corresponds to the σ-complex with the C_{TCNX}-O_{bridge} bond length equal to 1.38827 Å. The σ-complex structure shows largely split C≡N vibrational peaks and several C_{TCNX}-O_{bridge} vibrational peaks. Note that the C_{TCNX}-O_{bridge} vibrational peaks are attributed to coupled vibrational models of the C_{TCNX}-O_{bridge} bond and naphthalene ring. With increasing the C_{TCNX}-O_{bridge} bond length, the C≡N splitting is shrunk and C_{TCNX}-O_{bridge} vibrational peaks almost disappear at the bond lengths longer than 1.6 Å, similarly to [Ti(OH)$_3$(H$_2$O)$_2$O-TCNQ$^-$]. However, in contrast to the case of TCNQ, the experimental spectra (green dashed curves) observed for the TiO$_2$-1,4-TCNAQ complex are not in accordance with the calculated C≡N and C_{TCNX}-O_{bridge} vibrational spectra (blue curves) of the σ-complex (top spectra). The observed vibrational spectra are in good agreement with those of the structure with the C_{TCNX}-

Table 1. Dependences of wavelengths and configurations of the lowest electronic excitations in [Ti(OH)$_3$(H$_2$O)$_2$O-TCNQ$^-$] [Ti(OH)$_3$(H$_2$O)$_2$O-1,4-TCNAQ$^-$], and [Ti(OH)$_3$(H$_2$O)$_2$O-TCNTQ$^-$] on the C_{TCNX}-O_{bridge} bond length.

C_{TCNQ}-O_{bridge} bond lengths (Å)	[Ti(OH)$_3$(H$_2$O)$_2$O-TCNQ$^-$]	[Ti(OH)$_3$(H$_2$O)$_2$O-1,4-TCNAQ$^-$]	[Ti(OH)$_3$(H$_2$O)$_2$O-TCNTQ$^-$]
Optimal	497 nm HOMO→LUMO(100%)	544 nm HOMO→LUMO(100%)	570 nm HOMO→LUMO(100%)
1.6	485 nm HOMO→LUMO(99%)	523 nm HOMO→LUMO(99%)	507 nm HOMO→LUMO(99%)
1.8	548 nm HOMO→LUMO(100%)	571 nm HOMO→LUMO(100%)	530 nm HOMO→LUMO(100%)
2.0	557 nm HOMO→LUMO(100%)	563 nm HOMO→LUMO(100%)	523 nm HOMO→LUMO(100%)

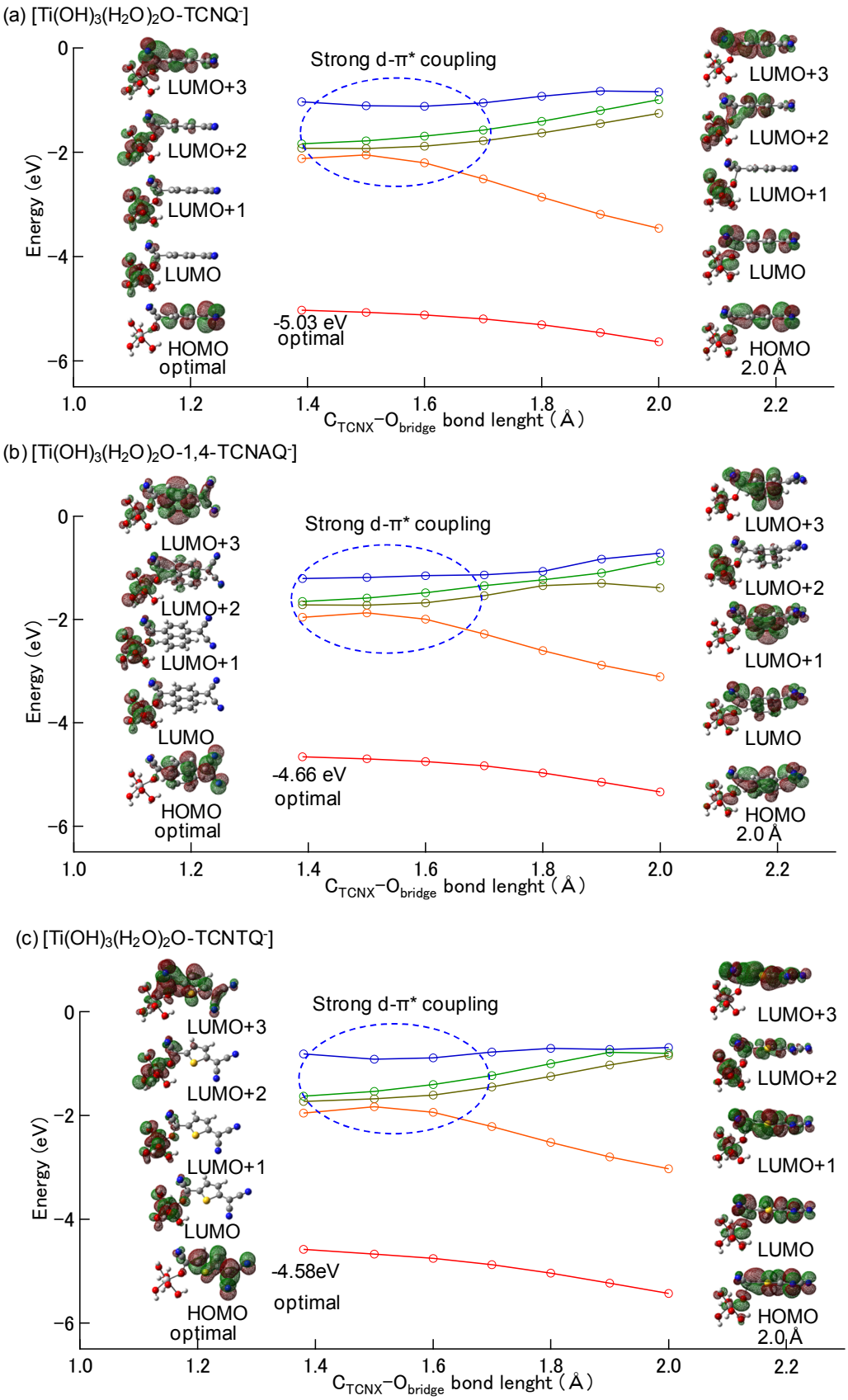

Fig. 8. Dependences of the energies and electronic distributions of HOMO (red), LUMO (orange), LUMO+1 (yellow), LUMO+2 (green), and LUMO+3 (blue) of (a) $[Ti(OH)_3(H_2O)_2O\text{-}TCNQ^-]$, (b) $[Ti(OH)_3(H_2O)_2O\text{-}1,4\text{-}TCNAQ^-]$, and (c) $[Ti(OH)_3(H_2O)_2O\text{-}TCNTQ^-]$ on the C_{TCNX}-O_{bridge} bond length. Green and brown isosurfaces stand for signs opposite in amplitude.

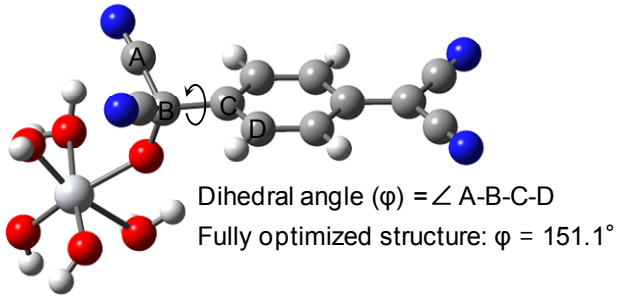

Fig. 9. Dihedral angle between the benzene ring and sp^3-type dicyanomethylene group in the fully optimized structure of $[Ti(OH)_3(H_2O)_2O\text{-}TCNQ^-]$.

O_{bridge} bond length equal to 2.0 Å. A similar result was obtained for TCNTQ. As shown in the left figure of Fig. 5(b), the fully optimized structures of $[Ti(OH)_3(H_2O)_2O\text{-}TCNTQ^-]$ is a σ-complex with the C_{TCNX}-O_{bridge} bond length equal to 1.38413 Å. The σ-complex structure shows largely split C≡N vibrational peaks and several C_{TCNX}-O_{bridge} vibrational peaks. The experimental spectra (red dashed curves) observed for the TiO_2-TCNTQ complex are not in coincidence with the calculated C≡N and C_{TCNX}-O_{bridge} vibrational spectra (blue curves). The observed vibrational spectra are in good agreement with those of the structure with the C_{TCNX}-O_{bridge} bond length equal to 2.0 Å. The optimized structures of $[Ti(OH)_3(H_2O)_2O\text{-}1,4\text{-}TCNAQ^-]$ and $[Ti(OH)_3(H_2O)_2O\text{-}TCNTQ^-]$ at 2.0 Å have no tetragonal conformation at the C_α atom without σ-bond with the bridging oxygen atom. These DFT analyses reveal that the complexes formed with 1,4-TCNAQ and TCNTQ correspond to weakly bonded complexes without the σ-bond formation.

Fig. 6(a)-6(c) show charge distributions in the fully optimized $[Ti(OH)_3(H_2O)_2O\text{-}TCNQ^-]$ and $[Ti(OH)_3(H_2O)_2O\text{-}1,4\text{-}TCNAQ^-]$ and $[Ti(OH)_3(H_2O)_2O\text{-}TCNTQ^-]$ optimized with the C_{TCNX}-O_{bridge} bond length of 2.0 Å. In the fully optimized $[Ti(OH)_3(H_2O)_2O\text{-}TCNQ^-]$, the total charge of the TCNQ moiety was calculated to be -1.199. This estimated charge is consistent with the σ-complex with a charge of -1, as shown in Fig. 1(b). On the other hand, the total charges of the TCNX moieties in $[Ti(OH)_3(H_2O)_2O\text{-}1,4\text{-}TCNAQ^-]$ and $[Ti(OH)_3(H_2O)_2O\text{-}TCNTQ^-]$ were estimated to be -0.671 and -0.703, respectively. This partial charge-transfer between TiO_2 and TCNX indicates that the weakly bonded complexes are assigned to charge-transfer complexes.

Next, we examined the visible-light absorption bands of the TiO_2-1,4-TCNAQ and -TCNTQ complexes by TD-DFT calculations. Fig. 7(a)-7(c) show calculated electronic-excitation spectra of $[Ti(OH)_3(H_2O)_2O\text{-}TCNQ^-]$, $[Ti(OH)_3(H_2O)_2O\text{-}1,4\text{-}TCNAQ^-]$ and $[Ti(OH)_3(H_2O)_2O\text{-}TCNTQ^-]$ with different C_{TCNX}-O_{bridge} bond lengths. For all the model complexes, similar bond-length dependences of electronic excitations are seen. The fully optimized structures that correspond to the σ-complexes show a relatively broad

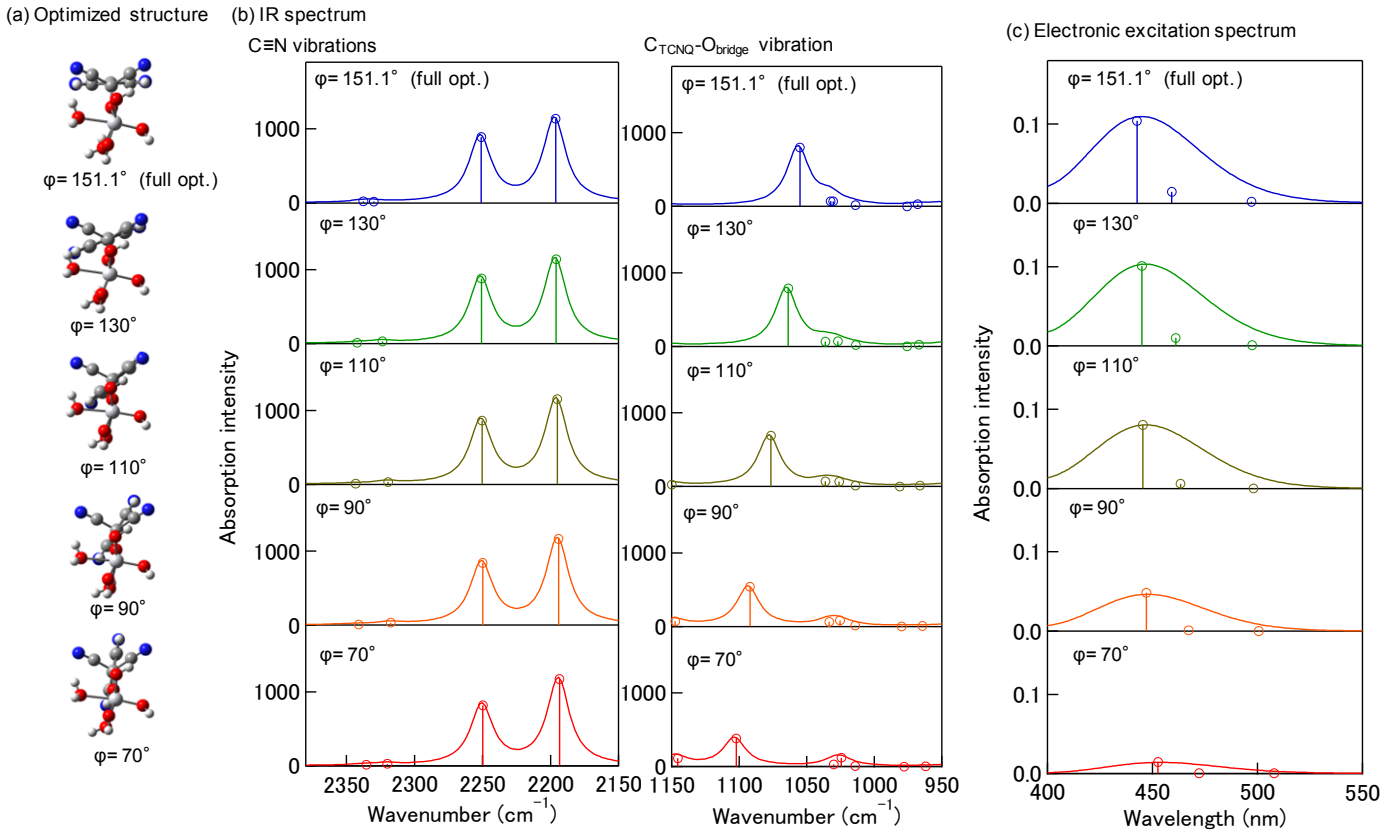

Fig. 10. (a) Optimized structures of $[Ti(OH)_3(H_2O)_2O\text{-}TCNQ^-]$ with different dihedral angles (φ), (b) their calculated vibrational absorption spectra, and (c) electronic-excitation spectra. The vibrational and electronic-excitation spectra were obtained by convolution of the line spectra with gaussian functions with FWHM of 20 and 3000 cm^{-1}, respectively.

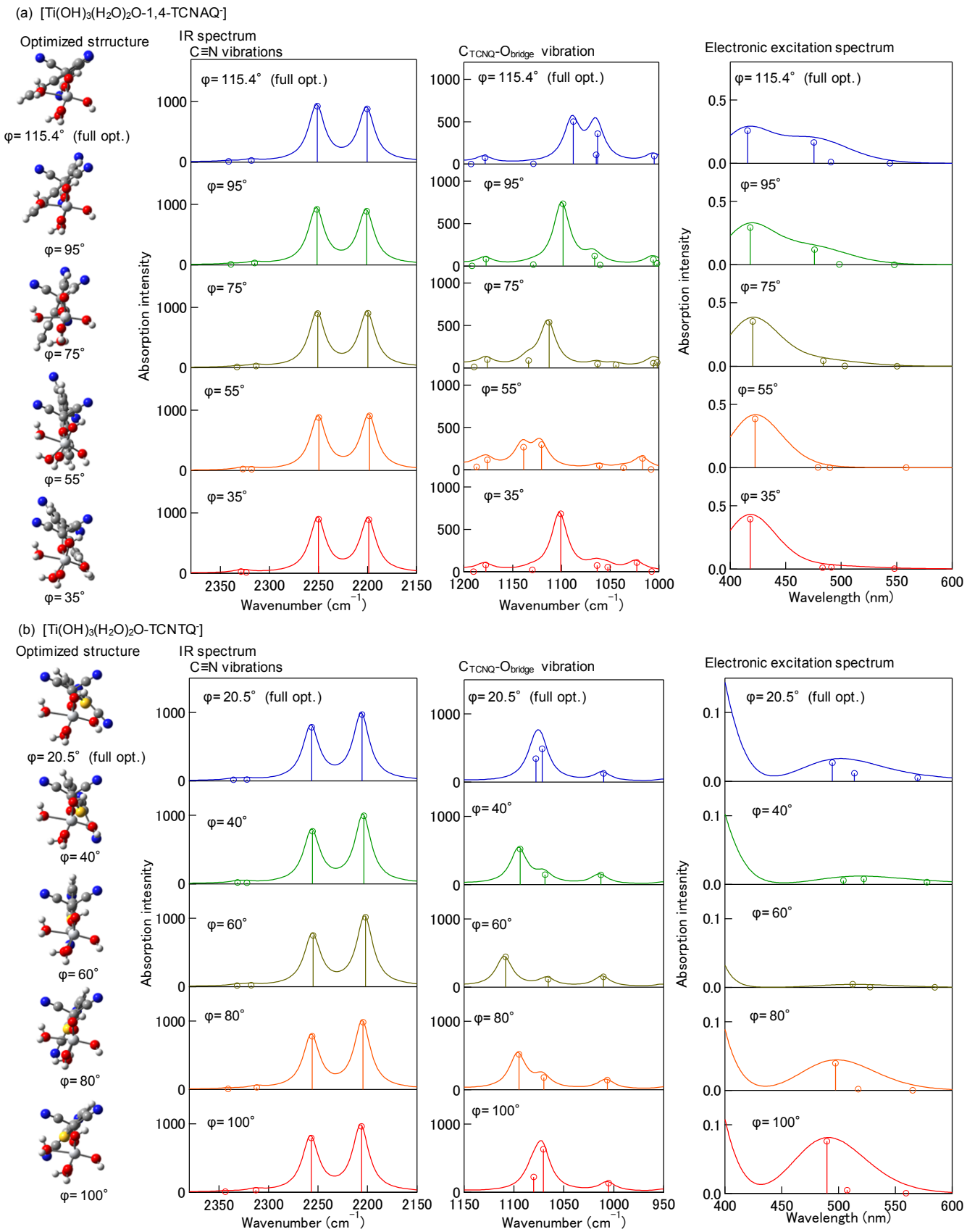

Fig. 11. Dependences of optimized structures, vibrational and electronic-excitation spectra on the dihedral angle (φ) in (a) $[Ti(OH)_3(H_2O)_2O\text{-}1,4\text{-}TCNAQ^-]$and (b) $[Ti(OH)_3(H_2O)_2O\text{-}TCNTQ^-]$. The vibrational and electronic-excitation spectra were obtained by convolution of the line spectra with gaussian functions with FWHM of 20 and 3000 cm^{-1}, respectively.

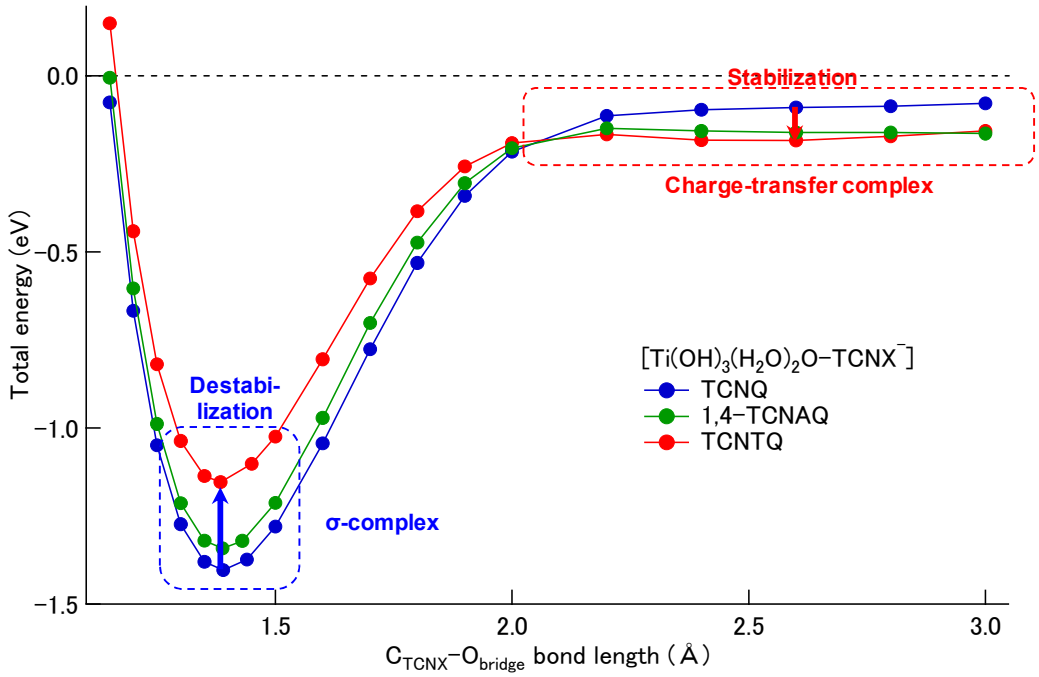

Fig. 12. Calculated potential curves of $[Ti(OH)_3(H_2O)_2O\text{-}TCNQ^-]$ (red), $[Ti(OH)_3(H_2O)_2O\text{-}1,4\text{-}TCNAQ^-]$ (green), and $[Ti(OH)_3(H_2O)_2O\text{-}TCNTQ^-]$ (blue) as a function of the C_{TCNQ}-O_{bridge} bond length.

absorption band in the visible region. With increasing the C_{TCNX}-O_{bridge} bond length, the absorption bands are red-shifted with the enhancement in the oscillator strength. In addition, the absorption bands become narrow. The optimized structures with $d_{C\text{-}O}$ = 2.0 Å that correspond to the charge-transfer complexes show a single strong electronic excitation in the visible region. As shown in Table 1, all the lowest electronic excitations in Fig. 7 are attributed to an electronic transition from the highest occupied molecular orbital (HOMO) to the lowest unoccupied molecular orbital (LUMO). Fig. 8(a)-8(c) shows the dependences of the energies and electronic distributions of HOMO, LUMO, and the second, third and forth lowest unoccupied molecular orbitals (LUMO+1, LUMO+2 and LUMO+3, respectively) in the model complexes on the C_{TCNX}-O_{bridge} bond length. In the σ-complexes with the bond length of 1.38-1.39 Å, the HOMO is distributed on the TCNX moiety and the LUMO, LUMO+1 and LUMO+2 on the Ti atom. Accordingly, the calculated electronic excitations (HOMO→LUMO, HOMO→LUMO+1 and HOMO→LUMO+2) in the visible region for the σ- complexes are assigned to ICT transitions. With increase in the C_{TCNX}-O_{bridge} bond length, avoided crossing between the 3d orbitals of the Ti atom and π* orbital of TCNX occurs with a large splitting, as reported in our recent paper.[8] In the charge-transfer complexes with the bond length equal to 2.0 Å, the HOMO and LUMO are delocalized on the TCNX and Ti-O_{bridge} moieties. Therefore, the single excitations in the charge-transfer complexes are assigned to interfacial electronic transitions with little charge-transfer nature between electronic states delocalized on TCNX and Ti-O_{bridge} moieties, which are different from the ICT transitions of the σ-complexes. It is noteworthy that the oscillator strengths of the interfacial non-charge-transfer transitions are more than one-order of magnitude higher than those of the ICT transitions in the σ-complexes. The enhancement in the transition probability results from the increase of the spatial overlap between HOMO and LUMO. As shown in Fig. 7(a), the broad absorption band (blue bashed curve) observed for the TiO_2-TCNQ σ-complex corresponds to the calculated ICT band (blue solid curve), although the absorption onset of the calculated spectrum is rather blue-shifted. This inconsistency in the onset energy results from the drawback of the mono-Ti complex that the energies of unoccupied orbitals of the model complex is significantly higher than the conduction band (ca. -4.0 eV vs a vacuum level) of TiO_2, as shown in Fig. 8(a). In fact, the reported TD-DFT calculations with a TiO_2 nanocluster well reproduced the absorption onset of the ICT band.[4,6] The relatively narrow absorption bands (green and red dashed curves) observed for the TiO_2-1,4-TCNAQ and -TCNTQ complexes are in good agreement with the calculated excitation spectra (orange curves) of the charge-transfer complexes with the C_{TCNX}-O_{bridge} bond length equal to 2.0 Å, as shown in Fig. 7(b) and 7(c). The lowest single strong interfacial non-charge-transfer excitations are consistent with the observed narrow absorption bands and relatively sharp rises in the TiO_2-1,4-TCNAQ and -TCNTQ complexes. Therefore, all the experimental and calculation results consistently support the formation of the charge-transfer complexes between TiO_2 and 1,4-TCNAQ and TCNTQ.

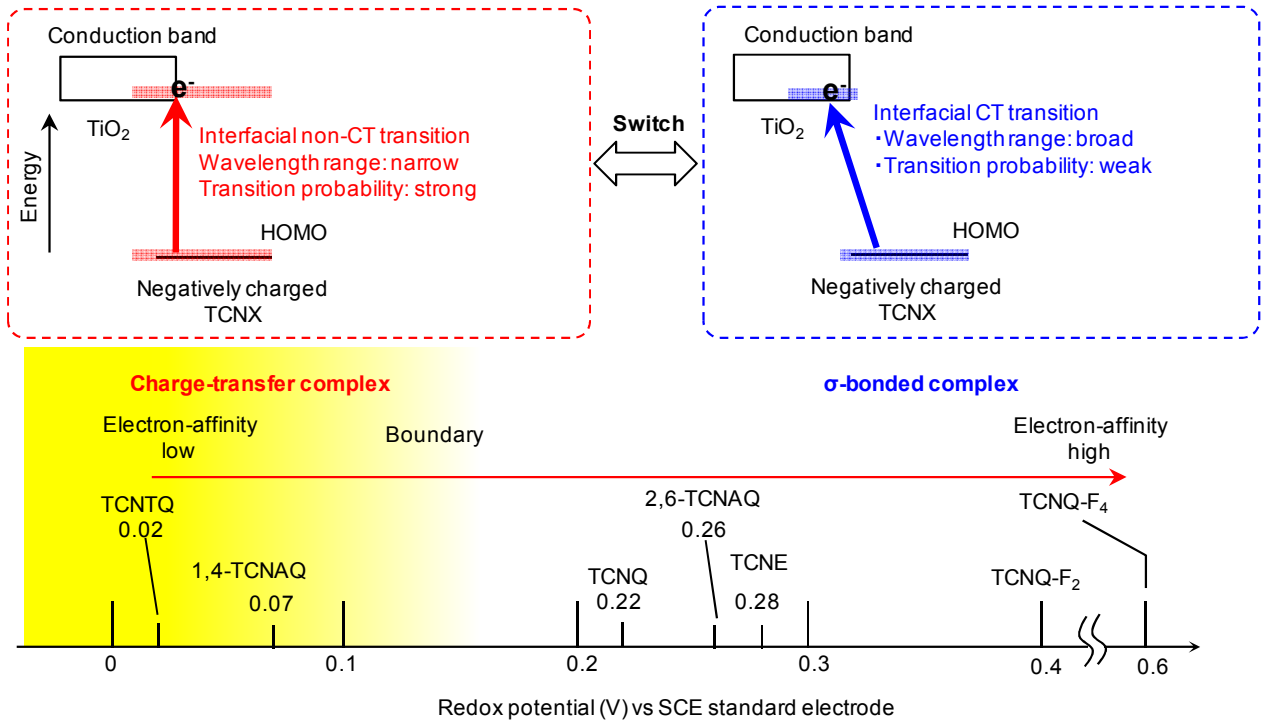

Fig. 13. Schematic diagram of two kinds of complex formations as a function of the redox potential of TCNX.

Effects of internal rotation of TCNX

In order to support the formation of the charge-transfer complexes, we should examine other possible structural changes than the C_{TCNX}-O_{bridge} bond. As shown in Fig. 9, the π-bond on the C_B-C_C bond between the benzene ring and dicyanomethylene group in TCNQ near the Ti-O_{bridge}-C_{TCNQ} bonding site is broken by the nucleophilic addition reaction. Consequently, the benzene moiety is considered to rotate about the C_B-C_C single bond at room temperature. Based on this consideration, we examined the effects of the internal rotation on the vibrational and electronic-excitation spectra. The internal rotation is described with the dihedral angle (φ) defined as shown in Fig. 9. For the fully optimized [$Ti(OH)_3(H_2O)$O-TCNQ$^-$] model complex, the dihedral angle is 151.1°. We calculated the optimized structures with different dihedral angles and their vibrational and electronic-excitation spectra, as shown in Fig. 10. In the structural optimizations, fortunately, the calculations were well converged without any restrictions of the coordinates of OH^- and H_2O ligands. Fig. 10(a) shows the optimized structures with different dihedral angles. Fig. 10(b) shows that the largely split C≡N vibrational peaks hardly change with decreasing the dihedral angle. In addition, the C_{TCNQ}-O_{bridge} vibrational mode is slightly blue-shifted and the intensity gradually decreases with the reduction of the dihedral angle, but never disappears. The absorption intensity of the ICT band in the visible region decreases with the dihedral angle, almost maintaining the excitation energies, as shown in Fig. 10(c). Similar dihedral-angle dependences of the vibrational and electronic-excitation spectra were obtained for the [$Ti(OH)_3(H_2O)$O-1,4-TCNAQ$^-$] and [$Ti(OH)_3(H_2O)$O-TCNTQ$^-$] model complexes, as shown in Fig. 11(a) and 11(b). The C≡N vibrational structures in the two model complexes are almost insensitive to the change in the dihedral angle. The wavenumbers and absorption intensities of the C_{TCNX}-O_{bridge} vibrational peaks change with the dihedral angle, but the peaks never disappear. This is reasonable because the C_{TCNX}-O_{bridge} σ-bond is maintained against the internal rotation. Therefore, the experimental results of the vibrational spectra of the TiO_2-1,4-TCNAQ and -TCNTQ complexes cannot be explained by the effects of the internal rotational. In addition, the narrow band-widths and sharp rises of the observed absorption bands cannot be reproduced by changing the dihedral angle. This result supports the formation of the charge-transfer complexes.

Stabilities of the charge-transfer complex and σ-complex

In order to further support the formation of the charge-transfer complexes, we examined the stabilities of the charge-transfer complex and σ-complex. Fig. 12 shows the potential curves of the three model complexes as a function of the C_{TCNX}-O_{bridge} bond length. There exist two complex states. The one is the σ-complex in the strong bonding region and the other is the charge-transfer complex in the weak bonding region. It is very interesting that the stability of the σ-complex is reduced with the electron affinity of TCNX from TCNQ to 1,4-TCNAQ, TCNTQ. On the other hand, the stability of the charge-transfer complex increases for 1,4-TCNAQ and TCNTQ. The potential curves for 1,4-TCNAQ and TCNTQ indicate that the σ-complex is energetically preferable to the charge-transfer

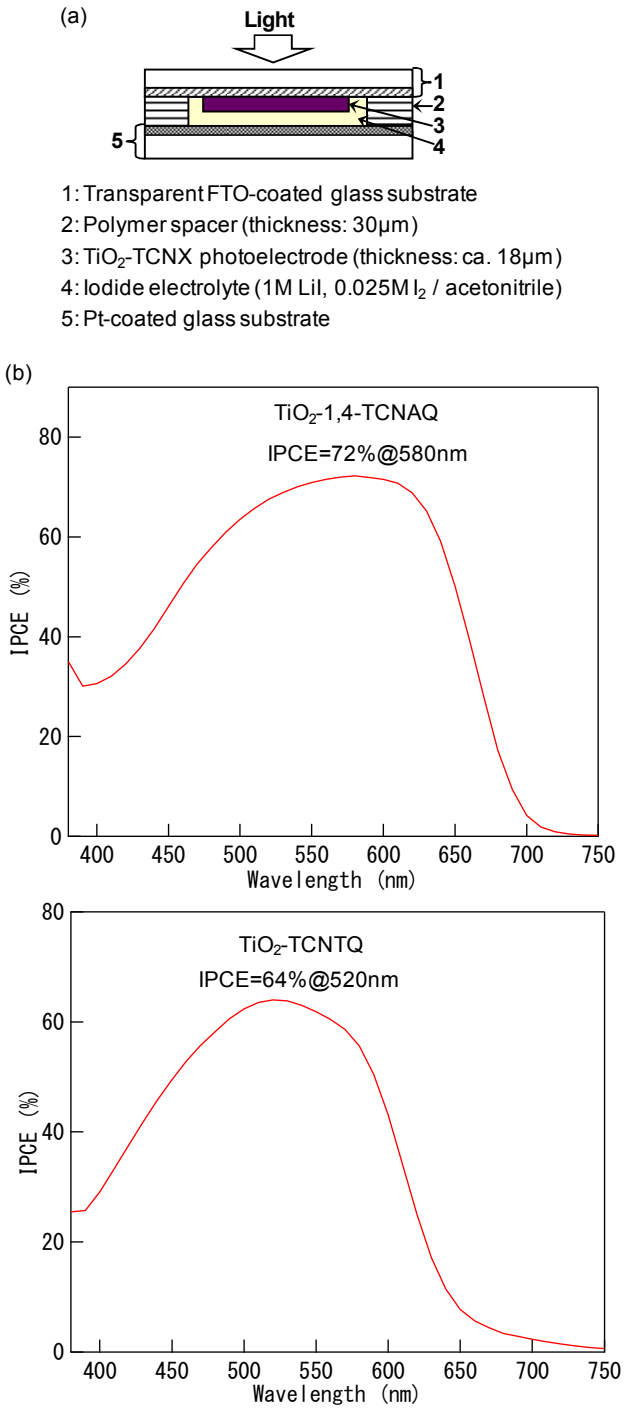

Fig. 14. (a) Schematic picture and (b) IPCE spectra of TiO_2-1,4-TCNAQ and TiO_2-TCNTQ based photovoltaic cells.

complex. There should be a certain reason to reduce the stability of the σ-complex as compared to the charge-transfer complex. In contrast to the charge-transfer complex, the formation of the σ-complex needs close contact with a TiO_2 surface. The steric hindrance by surface water molecules physically adsorbed on TiO_2 is likely to destabilize the σ-complex state especially for the weaker electron acceptors (1,4-TCNAQ and TCNTQ). In addition, we found that the stability of the σ-complex is significantly reduced by addition of a proton to the O_{bridge} atom. Together with complicate solvent effects, these factors are considered to destabilize the σ-complex for 1,4-TCNAQ and TCNTQ, leading to the preferable formation of the charge-transfer complex. In order to evaluate the stabilities of the two kinds of complexes more quantitatively, the use of TiO_2 nanoclusters instead of the mononuclear Ti model complexes is required. DFT calculations with a TiO_2 nanocluster are now in progress in our group.

Fig. 13 shows a diagram of the complexes formed between TiO_2 and TCNX as a function of the redox potential of TCNX including the σ-complex formation for TCNE (tetracyanoethylene), 2,6-TCNAQ (11,11,12,12-tetracyanonaphtho-2,6-quinodimethane), TCNQ-F_2 and TCNQ-F_4.[5,27] The features of the electronic transitions of the charge-transfer complex and σ-complex are summarized in the top of the figure. Our work demonstrates that the formations of the σ-complex and charge-transfer complex would be switched between +0.1 and +0.2 V and are selectively controlled with the electron affinity of TCNX. In this diagram, TCNQ is located around the boundary between the two complex states. This fact implies that the σ-complex state is switched to the charge-transfer complex state with little environmental changes such as solvent and temperature. Our recent research of solvent effects on the absorption spectrum of the TiO_2-TCNQ σ-complex indicates that the σ-complex might be switched to the charge-transfer complex.[27] This result will be reported elsewhere.

Light-energy conversion by the charge-transfer complexes

Finally, we examined the application of the charge-transfer complexes to photovoltaic conversions. We fabricated electrochemical photovoltaic cells by the method described in the Experimental section. The cell structure is depicted in Fig. 14(a). Fig. 14(b) shows excitation spectra of incident photon-to-current conversion efficiencies (IPCE) of the TiO_2-1,4-TCNAQ and TiO_2-TCNTQ based photovoltaic cells with iodide electrolyte. The former cell showed an IPCE maximum 72% at 580 nm and the latter one 64% at 520 nm. This result indicates that the charge-transfer complexes effectively work for photovoltaic conversions, demonstrating the high potential of the charge-transfer complexes in applications to light-energy conversions. In addition, the result experimentally shows that the unoccupied orbitals delocalized on TiO_2 and TCNX in Fig. 8 are higher in energy than the conduction band of TiO_2, as illustrated in Fig. 13.

Conclusion

We report on the formation of charge-transfer complexes between TiO_2 and bis(dicyanomethylene) electron acceptors with lower electron affinities than TCNQ. The charge-transfer complexes show a strong visible-light absorption band due to the interfacial non-charge-transfer transition whose initial and final states are delocalized on both the TCNX and TiO_2

moieties. The charge-transfer complexes efficiently induce light-to-current conversions due to the interfacial electronic transition. Furthermore, our work demonstrates that the formations of the charge-transfer and σ-complexes can be selectively controlled by adjusting the electron affinity of TCNX.

Acknowledgements

This research was partially supported by the Precursory Research for Embryonic Science and Technology (PRESTO) program of the Japan Science and Technology Agency (JST) and Grant-in-Aid for Exploratory Research (Grant Number: 25620054) of Japan Society for the Promotion of Science (JSPS).

Notes and references

[1]Graduate School of Science and Technology, Gunma University, 1-5-1 Tenjin-cho, Kiryu, Gunma, 376-8515, Japan. E-mail: jfujisawa@gunma-u.ac.jp

[2]Department of Industrial Chemistry, Faculty of Engineering, Tokyo University of Science, Ichigaya-Funagawara, Shinjuku-ku, Tokyo 162-0826, Japan.

1 H. Kisch, *Semiconductor Photocatalysis: Principles and Applications*, Wiley-VCH, 2014.
2 K. Kalyanasundaram, *Dye-Sensitized Solar Cells*, EPFL Press, 2010.
3 T. Kubo, J. Fujisawa and H. Segawa, *Electrochemistry*, 2009, **77**, 977.
4 R. Jono, J. Fujisawa, H. Segawa and K. Yamashita, *J. Phys. Chem. Letters*, 2011, 2, 1167.
5 S. Manzhos, R. Jono, K. Yamashita, J. Fujisawa, M. Nagata and H. Segawa, *J. Phys. Chem. C*, 2011, **115**, 21487.
6 R. Jono, J. Fujisawa, H. Segawa and K. Yamashita, *Phys. Chem. Chem. Phys*. 2013, **15**, 18584.
7 J. Fujisawa, *Phys. Chem. Chem. Phys.*, 2015, **17**, 12228.
8 J. Fujisawa and M. Hanaya, *Phys. Chem. Chem. Phys.*, 2015, **17**, 16285.
9 D. S. Acker and W. R. Hertler, *J. Am. Chem. Soc.*, 1962, **84**, 3370.
10 H. Hosaka, T. Fujiwara and K. Meguro, *Bull. Chem. Soc. Jpn*., 1971, **44**, 2616.
11 K. Esumi and K. Meguro, *Bull. Chem. Soc. Jpn*., 1982, **55**, 1647.
11 R.S. Mulliken, *J. Am. Chem. Soc.*, 1952, **74**, 811.
12 We measured the redox potentials of 1,4-TCNAQ and TCNTQ in acetonitrile by means of differential pulse voltammetry, using a Pt working and counter electrodes, a SCE (saturated calomel electrode) reference electrode, and tetra-*n*-butylammonium hexafluorophosphate as supporting electrolyte.
13 W. Kohn and L. J. Sham, *Phys. Rev*., 1965, **140**, A1133.
14 M. A. L. Marques and E. K. U. Gross. *Annu. Rev. Phys. Chem.* 2004, **55**, 427.
15 A.D. Becke, *J. Chem. Phys.*, 1993, **98**, 5648.
16 C. Lee, W. Yang and R. G. Parr, *Phys. Rev. B*, 1988, **37**, 785.
17 R. Ditchfield, W. Hehre and J. Pople, *J. Chem. Phys.*, 1971, **54**, 724.
18 W. Hehre, R. Ditchfield and J. Pople, *J. Chem. Phys.*, 1972, **56**, 2257.
19 V. Barone and M. Cossi, *J. Phys. Chem. A*, 1998, **102**, 1995.
20 M. Cossi, N. Rega, G. Scalmani and V. Barone, *J. Comput. Chem*., 2003, **24**, 669.
21 Y. Takano and K. N. Houk, *J. Chem. Theory Comput*., 2005, **1**, 70.
22 T. Yanai, D. P Tew and N. C Handy, *Chem. Phys. Lett*., 2004, **393**, 51.
23 M. J. Frisch *et al*. Gaussian 09, revision D.01; Gaussian, Inc.: Wallingford, CT, 2009.
24 J. Moser, S. Punchihewa, P. P. Infelta and M. Grätzel, *Langmuir*, 1991, **7**, 3012.
25 R. Rodriguez, M. A. Blesa and A. E. Regazzoni, *J. Colloid Interf. Sci.*, 1996, **177**, 122.
26 J. Fujisawa and M. Nagata, *Chem. Phys. Lett.*, 2015, **619**, 180.
27 J. Fujisawa, unpublished results.

